NANO · MICRO small

www.small-journal.com

Multiscale Hierarchical Design of a Flexible Piezoresistive Pressure Sensor with High Sensitivity and Wide Linearity Range

Jidong Shi, Liu Wang, Zhaohe Dai, Lingyu Zhao, Mingde Du, Hongbian Li, and Ying Fang**

Flexible piezoresistive pressure sensors have been attracting wide attention for applications in health monitoring and human-machine interfaces because of their simple device structure and easy-readout signals. For practical applications, flexible pressure sensors with both high sensitivity and wide linearity range are highly desirable. Herein, a simple and low-cost method for the fabrication of a flexible piezoresistive pressure sensor with a hierarchical structure over large areas is presented. The piezoresistive pressure sensor consists of arrays of microscale papillae with nanoscale roughness produced by replicating the lotus leaf's surface and spray-coating of graphene ink. Finite element analysis (FEA) shows that the hierarchical structure governs the deformation behavior and pressure distribution at the contact interface, leading to a quick and steady increase in contact area with loads. As a result, the piezoresistive pressure sensor demonstrates a high sensitivity of 1.2 kPa^{-1} and a wide linearity range from 0 to 25 kPa. The flexible pressure sensor is applied for sensitive monitoring of small vibrations, including wrist pulse and acoustic waves. Moreover, a piezoresistive pressure sensor array is fabricated for mapping the spatial distribution of pressure. These results highlight the potential applications of the flexible piezoresistive pressure sensor for health monitoring and electronic skin.

1. Introduction

The flexible pressure sensors that can be integrated with curved surfaces are attracting significant attention due to their promising applications in wearable health monitoring systems[1–4] and human-machine interfaces.[5–10] Rapid progress has been made in the development of flexible pressure sensors based on a variety of sensing mechanisms, including piezoresistivity,[11–14] piezoelectricity,[15–17] capacitance,[18–20] and triboelectricity.[3,21,22] In particular, piezoresistive pressure sensors have been widely adopted because of their simple device structure and easy signal processing.[23] A typical design of a flexible piezoresistive pressure sensor consists of two opposing elastomers coated with conductive electrodes. Under the stimuli of an applied pressure, the two elastomers come into contact to form conduction paths, transducing the applied pressure into a change in current. The flexible piezoresistive pressure sensors with both high sensitivity and wide linearity range are highly desirable for monitoring human physiological signals and body motions. For example, intracranial pressure and intraocular pressure in human are normally around 1 and 2 kPa, respectively.[24,25] On the other hand, a typical systolic pressure in human is between 13 and 26 kPa.[26] Besides, the pressure of human finger press and object manipulation is above 10 kPa.[27–30]

The performance of a flexible piezoresistive pressure sensor depends on the deformation behavior of both conducting electrodes and elastomers. Recently, nanomaterials such as graphene,[31] carbon nanotubes (CNTs),[32] and metal nanowires[33] have been intensively investigated as active electrode materials because of their mechanical flexibility. Furthermore, elastomers, such as polydimethylsiloxane (PDMS), have been engineered with a variety of surface microstructures,

J. D. Shi, L. Y. Zhao, M. D. Du, Prof. H. B. Li, Prof. Y. Fang
CAS Key Laboratory for Biomedical Effects of Nanomaterials and Nanosafety
CAS Center for Excellence in Nanoscience
National Center for Nanoscience and Technology
Beijing 100190, China
E-mail: lihb@nanoctr.cn; fangy@nanoctr.cn

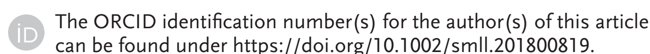
The ORCID identification number(s) for the author(s) of this article can be found under https://doi.org/10.1002/smll.201800819.

DOI: 10.1002/smll.201800819

J. D. Shi, L. Y. Zhao, M. D. Du, Prof. H. B. Li, Prof. Y. Fang
University of Chinese Academy of Sciences
Beijing 100049, China

L. Wang, Z. H. Dai
Center for Mechanics of Solids
Structures and Materials
Department of Aerospace Engineering and Engineering Mechanics
The University of Texas at Austin
Austin, TX 78712, USA

Prof. Y. Fang
CAS Center for Excellence in Brain Science and Intelligence Technology
320 Yue Yang Road, Shanghai 200031, China

© 2018 WILEY-VCH Verlag GmbH & Co. KGaA, Weinheim

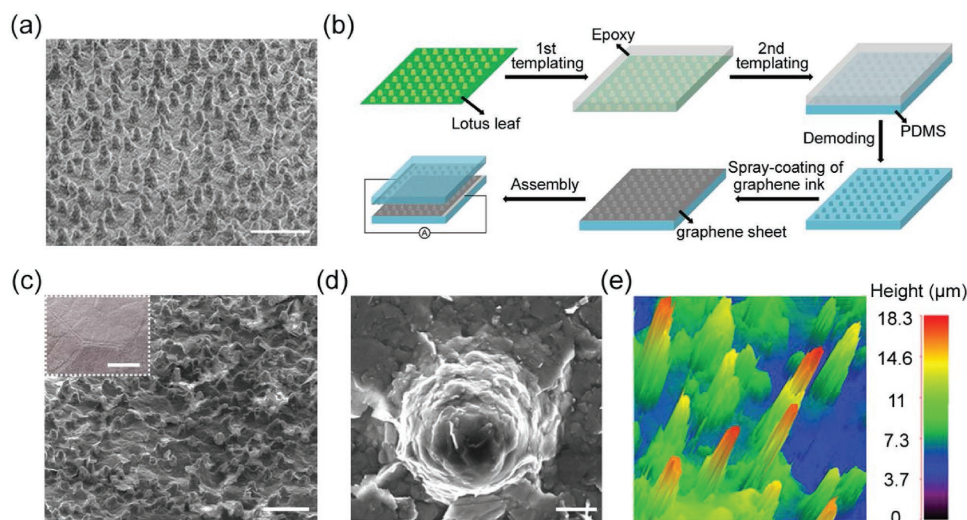

Figure 1. Flexible piezoresistive pressure sensor with a hierarchical structure. a) SEM image of a lotus leaf. Scale bar: 40 μm. b) Schematic illustration of the fabrication process of a pressure-sensor device. c) SEM image of a patterned graphene/PDMS. Scale bar: 50 μm. Inset: Photograph of the patterned graphene/PDMS. Scale bar: 5 mm. d) SEM image of a single papilla on the graphene/PDMS surface. Scale bar: 5 μm. e) 3D confocal image of the graphene/PDMS.

including micropyramids,[34] microdomes,[35] hollow-spheres,[36] and bionic microstructures[32,37–39] to increase their compressibility. In low pressure regime, these microstructures can concentrate loads effectively, leading to a quick increase in contact area with loads and therefore greatly improved sensitivity. However, with increased pressure, the incremental deformation and build-up of stress in pre-existing contact area leads to a decrease in sensitivity and consequently deviation from linearity. To date, few reported piezoresistive pressure sensors could sustain good linearity up to 3 kPa (Table S1, supporting information).

To extend the linearity range, flexible piezoresistive pressure sensors with complex surface structures have been designed and successfully demonstrated. For example, Bae et al. reported a highly sensitive piezoresistive pressure sensor with a wide linearity range from 0 to 12 kPa, by using a chemical vapour deposited-graphene/PDMS microdome array with wrinkled surface.[40] Shu et al. fabricated a flexible pressure sensor by using a piezoresistive nanocomposite with a Gaussian random distribution surface profile, increasing the upper limit of linearity to 14 kPa.[41] Despite the promise of these complex structures, there still lacks a facile and low-cost method to fabricate flexible piezoresistive pressure sensors with extended linearity.

Here, a hierarchical structure was fabricated by replicating the surface of lotus leaf onto PDMS substrates. Lotus leaf has a multiscale hierarchical surface, which endows the PDMS surface with both micro and nanoscale patterns. Sprayed graphene films were used as active electrodes. The as-prepared pressure sensor exhibits a wide linearity range from 0 to 25 kPa, with a sensitivity of 1.2 kPa^{-1}, a detection limit of 5 Pa, and great stability (>1000 cycles). FEA simulation shows that the hierarchical structure leads to a quick and steady increase in contact area with loads. The flexible piezoresistive pressure sensor has been demonstrated for the detection of wrist pulse, acoustic waves, and finger pressing. Moreover, a proof-of-concept pressure sensor array has been further demonstrated for the mapping of spatial pressure distribution.

2. Results and Discussions

As shown in the scanning electron microscopy (SEM) image in **Figure 1**a, the surface of a lotus leaf consists of randomly distributed microscale papillae decorated with nanoscale tomenta (Figure 1a; Figure S1a, Supporting Information).[42] A two-step molding process was used to transfer the surface structure of the lotus leaf to a PDMS positive replicate (Figure 1b).[37] First, a mixture of epoxy resin and curing agent was applied on the surface of the lotus leaf to create a negative mold (Figure S2, Supporting Information). After complete hardening of the epoxy resin, the lotus leaf and the negative epoxy mold were separated. Second, PDMS precursor and cross-linker were poured onto the epoxy mold and transferred to a vacuum chamber to facilitate PDMS infiltration. After curing, the positive PDMS replicate was peeled off from the negative mold. To obtain the active electrode, graphene ink, consisting of few-layer graphene flakes (Figures S3 and S4, Supporting Information), was spray-coated onto the patterned PDMS surface to form a continuous film. The thickness of the graphene electrode can be easily controlled by adjusting the concentration of the graphene ink and the coating time. As shown in Figure 1c, the papilla structure of the lotus leaf has been successfully transferred to the graphene/PDMS film. Figure 1d and Figure S5 (Supporting Information) show the enlarged SEM images of a single papilla with nanoscale roughness on the graphene/PDMS film. It can be seen that the stacked graphene flakes have completely covered the surface of PDMS. 3D confocal imaging shows that the height of the papillae on the graphene/PDMS film ranges from 7 to 18 μm and the average spacing between each papillae is ≈20 μm (Figure 1e; Figure S6, Supporting Information).

To construct a piezoresistive pressure-sensor device, two patterned graphene/PDMS films are stacked together face-to-face (Figure 1b). The current between the two electrodes was measured by applying a constant voltage of 0.2 V. In the absence of external pressure, the initial contact between the two graphene

© 2018 WILEY-VCH Verlag GmbH & Co. KGaA, Weinheim

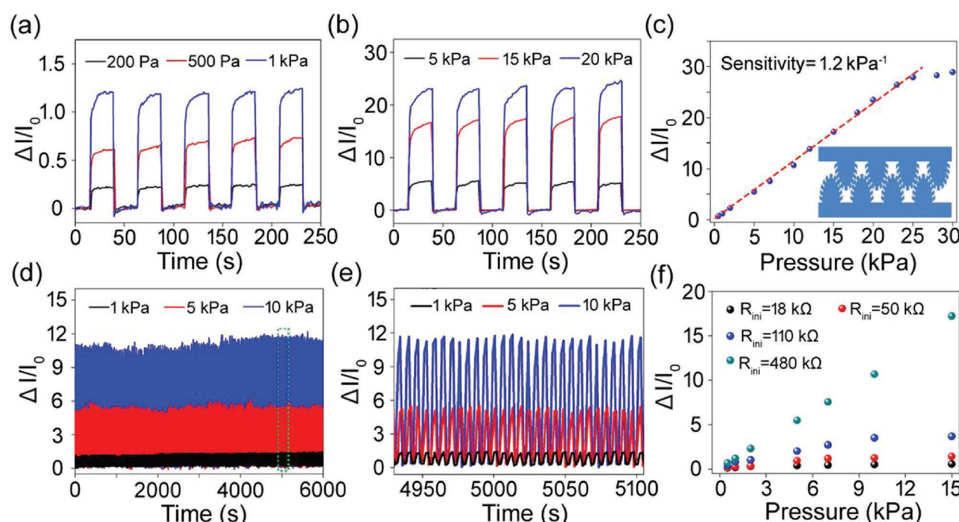

Figure 2. Pressure sensing performance of the patterned graphene/PDMS pressure-sensor devices. a,b) Real-time current response of a pressure-sensor device with an initial resistance of 480 kΩ. c) Sensitivity of the device from 0.2 to 25 kPa. Inset: Schematic of contact between two hierarchical graphene/PDMS films. d) Stability test (1000 cycles) under pressure of 1, 5, and 10 kPa. e) Magnified view of the dashed box in panel (d). f) Sensitivity of devices with different initial resistances.

electrodes is formed mainly at the tips of the papillae. The small contact area results in a large initial resistance, R_0, and a small initial current, I_0. By applying an external pressure, the graphene/PDMS films are compressed against each other, leading to an increase in contact area and, accordingly, an increase in device current. The sensitivity, S, of the device is defined as $S = (\Delta I/I_0)/P$, where ΔI is the change in device current and P is the applied pressure. **Figure 2**a–c shows the response of a pressure-sensor device, with an initial resistance of 480 kΩ, as a function of applied pressure ranging from 0.2 to 25 kPa. The device exhibited a high sensitivity of 1.2 kPa^{-1} and excellent linearity with a correlation coefficient of 0.998 (Figure 2c). Notably, the linearity range of the device was kept up to 25 kPa, which is a significant improvement compared with former studies (Table S1, Supporting Information). We further evaluated the stability of the pressure-sensor device by loading/unloading pressures of 1, 5, and 10 kPa for over 1000 cycles. As shown in Figure 2d,e, the device demonstrated an outstanding cyclic stability. The limit of detection (LOD) of the pressure-sensor device was also analyzed by loading small weights.[30,32,40,43] As shown in Figure S7 (Supporting Information), the device responded quickly to a pressure as low as 5 Pa, which makes it suitable for the sensitive detection of very low pressures.

By increasing the thickness of the graphene electrodes, pressure-sensor devices with different initial resistances were further constructed and characterized for pressure detection. As shown in Figure 2f, the sensitivity of the pressure-sensor devices decreases with the reduced initial resistance. The sensitivity was measured to be 0.42, 0.21, and 0.14 kPa^{-1} for devices with initial resistance of 110, 50, and 18 kΩ, respectively. The decreased sensitivity of the devices can be explained by the reduced surface roughness from thick graphene coating (Figure S8, supporting information). First, the reduced surface roughness leads to increased contact area between electrodes in the absence of applied pressure, which results in an increased initial current. Second, the compressibility of the pressure-sensor devices decreased with reduced surface roughness. We further fabricated a planar pressure-sensor device by spray-coating graphene flakes on the flat PDMS surface. Other parameters of the planar device were kept the same with those of the patterned graphene/PDMS device with an initial resistance of 480 kΩ. The planar device exhibited a sensitivity of 0.2 kPa^{-1}, which is six times lower than that of the patterned graphene/PDMS device (Figure S9, Supporting Information). These results confirm that the hierarchical surface structure plays an important role for the improved performance of the pressure-sensor devices.

To elucidate the effects of the surface structure on device performances, FEA was implemented to simulate the deformation process of the devices with different structures under applied pressure. A 3D FEA model was designed as follows: three hemispheres are built with neo-Hookean elasticity and external pressure is applied to push the top hemisphere downward to make contacts with the two bottom hemispheres and the bottom plate (**Figure 3**a). The structural hierarchy is included by adding nanodomes onto the hemispheres[44] (Figure 3b; Figure S10, Supporting Information). The hemispherical shape has been chosen for ease of analysis, but its characteristics are representative of three-dimensional surface asperities.[45,46] The distribution of contact pressure in the smooth and hierarchical structures upon loading is summarized in Figure 3c,d, by which the mapping of contact areas is also obtained (contact is built at places where the pressure >0). For the structure consisting of smooth hemispheres, the top hemisphere forms single-node contacts with the two bottom hemispheres and also the bottom plate (Figure 3c). Upon increasing the loads, the change of the contact area is mainly contributed by the compressive deformation of the hemisphere at the single-node contact regions. The contact pressure in the smooth structure is not uniformly distributed over the contact regions. The incremental deformation of the single-node contact regions results in the build-up of pressure in pre-existing

 © 2018 WILEY-VCH Verlag GmbH & Co. KGaA, Weinheim

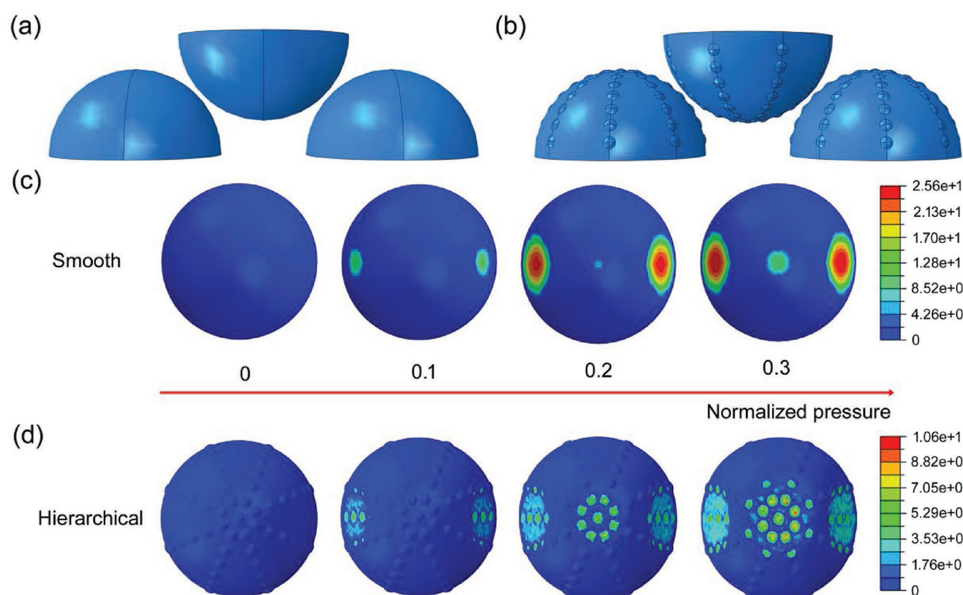

Figure 3. FEA modeling of the deformation process for smooth and hierarchical structures. a,b) Schematic illustrations for the contact of the smooth and hierarchical structure, respectively. c,d) Contact pressure distribution of the smooth and hierarchical structure, respectively, with increased applied pressure.

contact area, which leads to a deceleration in the increase of the contact area with loads (Figure S11, Supporting Information). As a result, the sensitivity decreases with increased pressure, leading to a deviation from linearity. For the hierarchical structure, the top hemisphere forms multinode contacts with the two bottom hemispheres and the bottom plate. As shown in Figure 3d, the number of the contact nodes increases quickly with loads because of the protruding nanodomes, leading to a quick increase in the contact area. In addition, the contact pressure in the hierarchical structure is more evenly distributed over the contact regions than that of the smooth structure. As a result, the contact area of the hierarchical structure increases more steadily than that of the smooth structure upon loading (Figure S11, Supporting Information). Since the change in current is proportional to the change in contact area,[40,41] pressure-sensor devices with hierarchical surface structures exhibit both high sensitivity and wide linearity range.

Our flexible pressure-sensor devices are wearable and can be applied for real-time health monitoring. Wrist pulse can provide useful and important information about the human health condition.[47,48] For example, cardiovascular diseases have been shown to be closely related with the shape of the wrist pulse waveform.[20,49] As shown in **Figure 4**a, a flexible pressure-sensor device was attached onto the radial artery of an adult human wrist to detect the pulse signals. Figure 4b presents the real-time recording of the pulse signals by the device. The corresponding heart rates were determined to be ≈78 beats min^{-1}. The pulse signals were also collected after exercise, where a heart rate of ≈93 was obtained (Figure S12, Supporting Information). Figure 4c illustrates a typical pulse waveform in which three peaks, including percussion wave (P1), tidal wave (P2), and diastolic wave (P3), can be clearly identified. We note that further improvement in resolution is needed for accurate biomedical diagnostics.

The flexible pressure-sensor devices can also be used for voice recognition. As shown in Figure 4d, a pressure-sensor device was attached onto a loud speaker.[50,51] The words/phrases "NCNST," "Graphene," "Pressure sensor," and "Lotus leaf" were played in sequence. The device was able to discriminate the vibration patterns from different words/phrases. Moreover, Figure 4e shows the reliable response of the device when the same phrase "Pressure sensor" was repeated five times. In addition to small pressures, the flexible pressure-sensor device can also be applied to detect finger pressing. As shown in Figure S13 (Supporting Information), a flexible pressure-sensor device was connected in series with a light emitting diode (LED).[52] The brightness of the LED was controlled by the pressure loaded on the device. As a result, it allowed vision-based detection of increased finger pressing (Movie S1, Supporting Information).

For many practical purposes, it is required to integrate the pressure-sensor devices into a pixel array for spatially resolved pressure measurements.[11,53–56] **Figure 5**a shows a flexible pressure sensor array of 3 × 3 pixels. Each pixel has an area of 3 mm × 3 mm, and the center-to-center distance between adjacent pixels is 4.5 mm. To evaluate the performance of the pressure sensor array, metal blocks with different shapes were placed on it. The pixels under the metal blocks were compressed, leading to localized current signals. As shown in Figure 5b,c, the pressure distribution patterns corresponding to different metal blocks were obtained by the pressure sensor array. In addition, the pressure sensor array could also be applied for continuous pressure mapping. Figure 5d shows the time-series response of the pressure sensor array when the number "7" was written on it with a glass rod. These results highlight the promising applications of the flexible piezoresistive pressure sensor in human-machine interfaces.

© 2018 WILEY-VCH Verlag GmbH & Co. KGaA, Weinheim

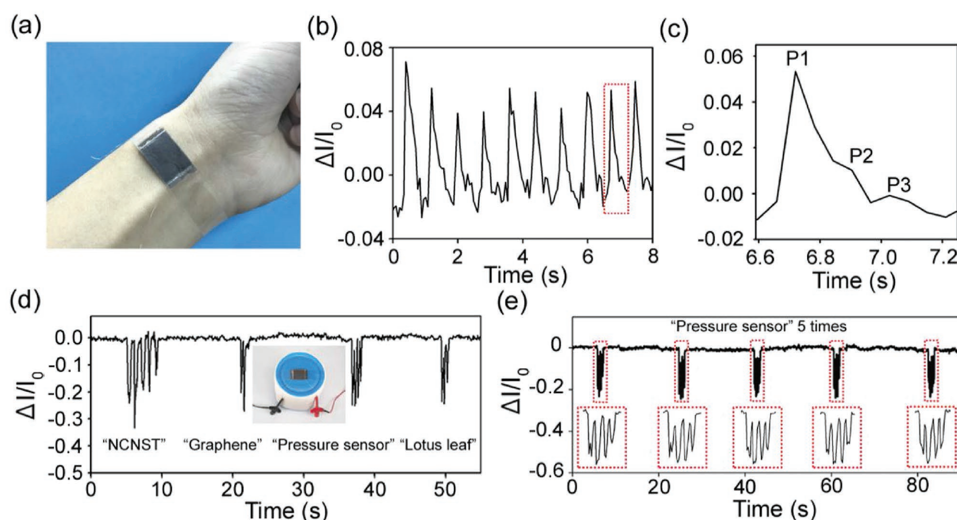

Figure 4. Flexible pressure sensor for monitoring wrist pulse and acoustic vibration. a) Photograph of a pressure-sensor device attached on the wrist. b) Real-time recording of wrist pulses. c) Magnified view of a single pulse. d) Response of a pressure-sensor device to acoustic vibration. Inset: Photograph of the pressure-sensor device attached onto a loud speaker. e) Response to repeated phrase "pressure sensor."

3. Conclusion

In summary, we have developed a facile and scalable method to fabricate a flexible piezoresistive pressure sensor with a hierarchical surface structure. The flexible pressure sensor exhibits a high sensitivity of 1.2 kPa^{-1} and a wide linearity range from 0 to 25 kPa, with excellent stability. As a result, the pressure sensor has been applied for sensitive measurements of wrist pulse, acoustic vibration, and finger press. A proof-of-concept pressure sensor array was further demonstrated for mapping of both static and dynamic pressure distribution. The ease of fabrication, high sensitivity, and wide linearity of the flexible piezoresistive pressure sensor make it a promising candidate in health monitoring and human-machine interfaces.

4. Experimental Section

Preparation of Flexible Piezoresistive Pressure Sensor: Epoxy base and curing agent were mixed (3:1 by weight) with a mechanical stirring process. After degassing, the mixture was poured onto a piece of lotus

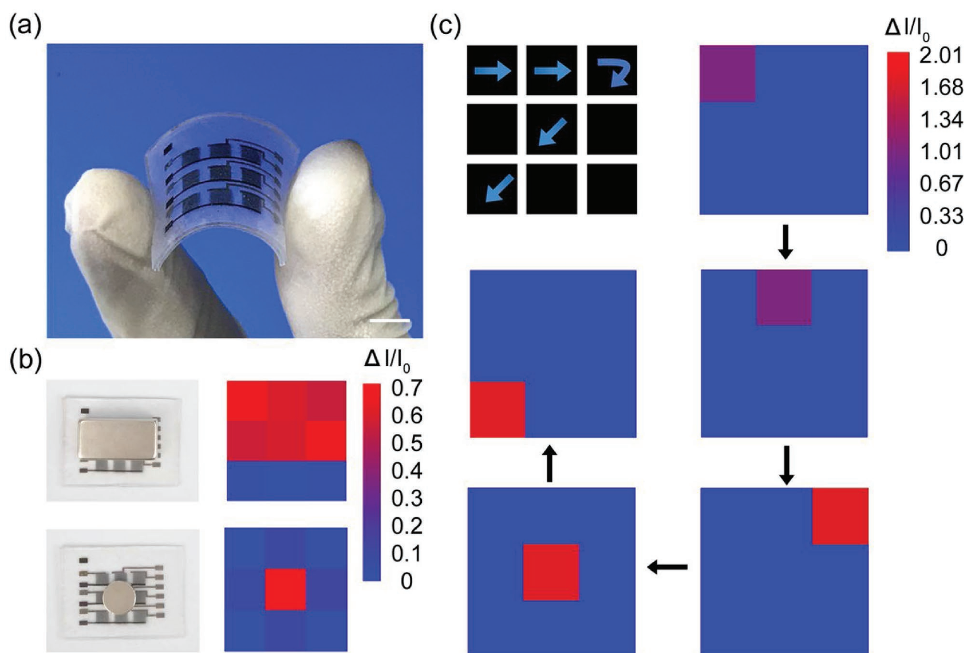

Figure 5. Flexible piezoresistive pressure sensor array for static and dynamic pressure mapping. a) Photograph of a flexible pressure sensor array. Scale bar: 5 mm. b) Response of the pressure sensor array to a square (top) and a round (bottom) metal block. c) Time-series response of the pressure sensor array as the number "7" was written on it.

© 2018 WILEY-VCH Verlag GmbH & Co. KGaA, Weinheim

leaf (collected in the Campus Lake of Beihang University) and cured at room temperature. After peeling off the lotus leaf, a negative epoxy mold was obtained. PDMS precursor (base: curing agent = 10:1 by weight, degassed) was then poured onto the negative epoxy mold. After vacuuming and curing at 60 °C for 2 h, the positive PDMS replicate was peeled off from the epoxy mold. A flexible electrode was prepared by spray coating graphene ink (Nanjing XFNano Materials Tech Co. Ltd, 101455) onto the patterned PDMS. The thickness of the graphene film was controlled by adjusting the spray time and the concentration of the graphene ink. A pressure sensor was fabricated by assembling two as-prepared flexible graphene/PDMS films face-to-face.

Preparation of Flexible Piezoresistive Pressure Sensor Array: The 3 × 3 piezoresistive pressure sensor array was prepared by assembling two PDMS elastomers with specially designed electrodes and graphene pads (Figure S14, Supporting Information). For each PDMS elastomer, the electrodes were fabricated by evaporating a gold layer of 100 nm in thickness under a shadow mask, and the graphene pads were prepared by spray-coating graphene ink with a shadow mask.

Structure Characterizations: Surface characterizations were conducted by a SEM (Nova 430). The distribution of surface heights was obtained by a confocal microscopy (Olympus, LEXT OLS4100). Raman spectrum of the graphene sheet was obtained by a Raman spectrometer (Renishaw inVia plus at 514.5 nm laser). Atomic force microscopy (AFM) analysis was conducted by a scanning probe microscopy (Veeco, Dimension 3100).

Testing of Pressure Sensing Performance: Pressure was applied by a dynamic mechanical analyzer (DMA, TA Q800). Current was recorded by a Keithley 4200-SCS semiconductor parameter analyzer. The low detection limit was analyzed by placing a small mass (100 mg) onto a pressure-sensor device (2 cm^{-2} in area).

FEA Simulation: FEA was implemented by using commercial package ABAQUS/Explicit 6.13. The hemispheres have a radius of $R = 50$, and center-to-center distance between the two lower hemispheres is $d = 3R$. In the hierarchical structure, 57 small spherical domes ($r = 5.5$) were added on the surface of each hemisphere (Figure S9, Supporting Information). Neo-Hookean material property with bulk/shear modulus ratio $K/G = 100$ was assigned to hemispheres and spherical domes. Frictionless contact interactions are assumed. The contact area was normalized by $A = \pi R^2$ and the applied force was normalized by $G \times A$.

Participants: Informed consent was obtained from Jidong Shi who volunteered to perform these studies. All testing reported conformed to the ethical requirements of the National Center for Nanoscience and Technology.

Supporting Information

Supporting Information is available from the Wiley Online Library or from the author.

Acknowledgements

Y.F. acknowledges supports from the National Natural Science Foundation of China (Grant No. 21673057), the International Co-operation Program of the Chinese Academy of Sciences (Grant No. 121D11KYSB20150022), and the Beijing Municipal Science and Technology Commission (Grant No. Z161100002116010). H.L. acknowledges support from the National Key R&D Program of China (Grant No. 2017YFF0209900, 2017YFF0209901). The authors thank Kailun Xia and Muqiang Jian from Tsinghua University; Shouliang Guan and Lei Gao from National Center for Nanoscience and Technology; Prof. Xuchun Gui from Sun Yet-sen University for helpful discussion. And we thank Yunsong Wang from Peking University for his kind help for the TEM characterization.

Note: The page numbers in references 5 and 13 were updated on July 5, 2018 after initial online publication.

Conflict of Interest

The authors declare no conflict of interest.

Keywords

graphene, hierarchical structure, linearity range, piezoresistive, pressure sensors

Received: March 1, 2018
Revised: April 17, 2018
Published online: May 30, 2018

[1] A. Chortos, J. Liu, Z. Bao, *Nat. Mater.* **2016**, *15*, 937.
[2] M. L. Hammock, A. Chortos, B. C. K. Tee, J. B. H. Tok, Z. Bao, *Adv. Mater.* **2013**, *25*, 5997.
[3] Z. Chen, Z. Wang, X. Li, Y. Lin, N. Luo, M. Long, N. Zhao, J. B. Xu, *ACS Nano* **2017**, *11*, 4507.
[4] X. Li, T. Yang, Y. Yang, J. Zhu, L. Li, F. E. Alam, X. Li, K. Wang, H. Cheng, C. Lin, Y. Fang, H. Zhu, *Adv. Funct. Mater.* **2016**, *26*, 1322.
[5] J. Shi, X. Li, H. Cheng, Z. Liu, L. Zhao, T. Yang, Z. Dai, Z. Cheng, E. Shi, L. Yang, Z. Zhang, A. Cao, H. Zhu, Y. Fang, *Adv. Funct. Mater.* **2016**, *26*, 2078.
[6] C. S. Boland, U. Khan, C. Backes, A. O'Neill, J. Mccauley, S. Duane, R. Shanker, Y. Liu, I. Jurewicz, A. B. Dalton, J. N. Coleman, *ACS Nano* **2014**, *8*, 8819.
[7] W. Yang, J. Chen, X. Wen, Q. Jing, J. Yang, Y. Su, G. Zhu, W. Wu, Z. L. Wang, *ACS Appl. Mater. Interfaces* **2014**, *6*, 7479.
[8] S. Jung, J. H. Kim, J. Kim, S. Choi, J. Lee, I. Park, T. Hyeon, D. H. Kim, *Adv. Mater.* **2014**, *26*, 4825.
[9] S. Lim, D. Son, J. Kim, Y. B. Lee, J. K. Song, S. Choi, D. J. Lee, J. H. Kim, M. Lee, T. Hyeon, *Adv. Funct. Mater.* **2015**, *25*, 375.
[10] C. Wang, D. Hwang, Z. Yu, K. Takei, J. Park, T. Chen, M. Ma, A. Javey, *Nat. Mater.* **2013**, *12*, 899.
[11] Y. Wei, S. Chen, Y. Lin, Z. Yang, L. Liu, *J. Mater. Chem. C* **2015**, *3*, 9594.
[12] M. Liu, X. Pu, C. Jiang, T. Liu, X. Huang, L. Chen, C. Du, J. Sun, W. Hu, Z. L. Wang, *Adv. Mater.* **2017**, *29*, 1703700.
[13] S. Gong, W. Schwalb, Y. Wang, Y. Chen, Y. Tang, J. Si, B. Shirinzadeh, W. Cheng, *Nat. Commun.* **2014**, *5*, 3132.
[14] C. Luo, N. Liu, H. Zhang, W. Liu, Y. Yue, S. Wang, J. Rao, C. Yang, J. Su, X. Jiang, Y. Gao, *Nano Energy* **2017**, *41*, 527.
[15] K. I. Park, J. H. Son, G. T. Hwang, C. K. Jeong, J. Ryu, M. Koo, I. Choi, S. H. Lee, M. Byun, Z. L. Wang, *Adv. Mater.* **2014**, *26*, 2514.
[16] K.-Y. Shin, J. S. Lee, J. Jang, *Nano Energy* **2016**, *22*, 95.
[17] S. Xu, Y. Qin, C. Xu, Y. Wei, R. Yang, Z. L. Wang, *Nat. Nanotechnol.* **2010**, *5*, 366.
[18] C. M. Boutry, A. Nguyen, Q. O. Lawal, A. Chortos, S. Rondeau-Gagné, Z. Bao, *Adv. Mater.* **2015**, *27*, 6954.
[19] L. Viry, A. Levi, M. Totaro, A. Mondini, V. Mattoli, B. Mazzolai, L. Beccai, *Adv. Mater.* **2014**, *26*, 2659.
[20] C. Pang, J. H. Koo, A. Nguyen, J. M. Caves, M. G. Kim, A. Chortos, K. Kim, P. J. Wang, J. B. H. Tok, Z. Bao, *Adv. Mater.* **2015**, *27*, 634.
[21] W. Wu, X. Wen, Z. L. Wang, *Science* **2013**, *340*, 952.
[22] L. Lin, Y. Xie, S. Wang, W. Wu, S. Niu, X. Wen, Z. L. Wang, *ACS Nano* **2013**, *7*, 8266.
[23] N. N. Jason, M. D. Ho, W. Cheng, *J. Mater. Chem. C* **2017**, *5*, 5845.
[24] M. Czosnyka, J. D. Pickard, *J. Neurol. Neurosurg. Psychiatry* **2004**, *75*, 813.
[25] M. J. Doughty, M. L. Zaman, *Surv. Ophthalmol.* **2000**, *44*, 367.

© 2018 WILEY-VCH Verlag GmbH & Co. KGaA, Weinheim

[26] A. V. Chobanian, G. L. Bakris, H. R. Black, W. C. Cushman, L. A. Green, J. L. Izzo Jr., D. W. Jones, B. J. Materson, S. Oparil, J. T. Wright Jr., *JAMA* **2003**, *289*, 2560.
[27] S. C. Mannsfeld, B. C. Tee, R. M. Stoltenberg, C. V. H. Chen, S. Barman, B. V. Muir, A. N. Sokolov, C. Reese, Z. Bao, *Nat. Mater.* **2010**, *9*, 859.
[28] Y. Zang, F. Zhang, C.-a. Di, D. Zhu, *Mater. Horiz.* **2015**, *2*, 140.
[29] T. Q. Trung, N. E. Lee, *Adv. Mater.* **2016**, *28*, 4338.
[30] S. H. Cho, S. W. Lee, S. Yu, H. Kim, S. Chang, D. Kang, I. Hwang, H. S. Kang, B. Jeong, E. H. Kim, *ACS Appl. Mater. Interfaces* **2017**, *9*, 10128.
[31] W. Chen, X. Gui, B. Liang, R. Yang, Y. Zheng, C. Zhao, X. Li, H. Zhu, Z. Tang, *ACS Appl. Mater. Interfaces* **2017**, *9*, 24111.
[32] X. Wang, Y. Gu, Z. Xiong, Z. Cui, T. Zhang, *Adv. Mater.* **2014**, *26*, 1336.
[33] Y. Wei, S. Chen, X. Dong, Y. Lin, L. Liu, *Carbon* **2017**, *113*, 395.
[34] C. L. Choong, M. B. Shim, B. S. Lee, S. Jeon, D. S. Ko, T. H. Kang, J. Bae, S. H. Lee, K. E. Byun, J. Im, *Adv. Mater.* **2014**, *26*, 3451.
[35] J. Park, Y. Lee, J. Hong, M. Ha, Y. D. Jung, H. Lim, S. Y. Kim, H. Ko, *ACS Nano* **2014**, *8*, 4689.
[36] L. Pan, A. Chortos, G. Yu, Y. Wang, S. Isaacson, R. Allen, Y. Shi, R. Dauskardt, Z. Bao, *Nat. Commun.* **2014**, *5*, 3002.
[37] M. Jian, K. Xia, Q. Wang, Z. Yin, H. Wang, C. Wang, H. Xie, M. Zhang, Y. Zhang, *Adv. Funct. Mater.* **2017**, *27*, 1606066.
[38] B. Su, S. Gong, Z. Ma, L. W. Yap, W. Cheng, *Small* **2015**, *11*, 1886.
[39] P. Nie, R. Wang, X. Xu, Y. Cheng, X. Wang, L. Shi, J. Sun, *ACS Appl. Mater. Interfaces* **2017**, *9*, 14911.
[40] G. Y. Bae, S. W. Pak, D. Kim, G. Lee, D. H. Kim, Y. Chung, K. Cho, *Adv. Mater.* **2016**, *28*, 5300.
[41] Y. Shu, H. Tian, Y. Yang, C. Li, Y. Cui, W. Mi, Y. Li, Z. Wang, N. Deng, B. Peng, T. Ren, *Nanoscale* **2015**, *7*, 8636.
[42] W. Barthlott, C. Neinhuis, *Planta* **1997**, *202*, 1.
[43] S. Liu, X. Wu, D. Zhang, C. Guo, P. Wang, W. Hu, X. Li, X. Zhou, H. Xu, C. Luo, J. Zhang, J. Chu, *ACS Appl. Mater. Interfaces* **2017**, *9*, 24148.
[44] J. F. Archard, *Proc. R. Soc. A* **1957**, *243*, 190.
[45] A. Yu, A. Liu, Q. Zhang, H. Hosseini, *J. Micromech. Microeng.* **2006**, *16*, 2157.
[46] Y.-P. Zhao, G.-C. Wang, T.-M. Lu, G. Palasantzas, J. T. M. De Hosson, *Phys. Rev. B* **1999**, *60*, 9157.
[47] W. W. Nichols, *Am. J. Hypertens.* **2005**, *18*, 3.
[48] Z. Wang, S. Wang, J. Zeng, X. Ren, A. J. Y. Chee, B. Y. S. Yiu, W. C. Chung, Y. Yang, A. C. H. Yu, R. C. Roberts, A. C. O. Tsang, K. W. Chow, P. K. L. Chan, *Small* **2016**, *12*, 3827.
[49] T. Yang, X. Jiang, Y. Zhong, X. Zhao, S. Lin, J. Li, X. Li, J. Xu, Z. Li, H. Zhu, *ACS Sensors* **2017**, *2*, 967.
[50] T. Yang, X. Li, X. Jiang, S. Lin, J. Lao, J. Shi, Z. Zhen, Z. Li, H. Zhu, *Mater. Horiz.* **2016**, *3*, 248.
[51] J. Shi, J. Hu, Z. Dai, W. Zhao, P. Liu, L. Zhao, Y. Guo, T. Yang, L. Zou, K. Jiang, H. Li, Y. Fang, *Carbon* **2017**, *123*, 786.
[52] W. Liu, N. Liu, Y. Yue, J. Rao, F. Cheng, J. Su, Z. Liu, Y. Gao, *Small14*, **2018**, 1704149.
[53] T. Yang, W. Wang, H. Zhang, X. Li, J. Shi, Y. He, Q. S. Zheng, Z. Li, H. Zhu, *ACS Nano* **2015**, *9*, 10867.
[54] S. Z. Guo, K. Qiu, F. Meng, S. H. Park, M. C. McAlpine, *Adv. Mater.* **2017**, *29*, 1701218.
[55] W. Liu, N. Liu, Y. Yue, J. Rao, C. Luo, H. Zhang, C. Yang, J. Su, Z. Liu, Y. Gao, *J. Mater. Chem. C* **2018**, *6*, 1451.
[56] H. Zhang, N. Liu, Y. Shi, W. Liu, Y. Yue, S. Wang, Y. Ma, L. Wen, L. Li, F. Long, Z. Zou, Y. Gao, *ACS Appl. Mater. Interfaces* **2016**, *8*, 22374.

© 2018 WILEY-VCH Verlag GmbH & Co. KGaA, Weinheim